Superconductor Vortex Spectrum Including Fermi Arc States in Time-Reversal Symmetric Weyl Semimetals

Rauf Giwa[1] and Pavan Hosur[1,2]
[1]University of Houston, Houston, Texas 77204, USA
[2]Texas Center for Superconductivity at the University of Houston, Houston, Texas 77204, USA

(Received 28 August 2022; revised 21 December 2022; accepted 27 March 2023; published 14 April 2023)

Using semiclassics to surmount the hurdle of bulk-surface inseparability, we derive the superconductor vortex spectrum in nonmagnetic Weyl semimetals and show that it stems from the Berry phase of orbits made of Fermi arcs on opposite surfaces and bulk chiral modes. Tilting the vortex transmutes it between bosonic, fermionic, and supersymmetric, produces periodic peaks in the density of states that signify novel nonlocal Majorana modes, and yields a thickness-independent spectrum at magic "magic angles." We propose (Nb,Ta)P as candidate materials and tunneling spectroscopy as the ideal experiment.

DOI: 10.1103/PhysRevLett.130.156402

Superconductor vortices are fundamentally quantum mechanical entities with discrete energy levels whose structure encodes properties of the parent superconductor and the normal metal. For instance, an ordinary Fermi gas and conventional superconductivity lead to a gapped vortex spectrum [1] while vortices in two dimensional (2D) spinless $p+ip$ superconductors [2] and s-wave superconductors that descend from a 2D Dirac fermion [3] host zero energy states known as Majorana modes (MMs). MMs are exotic states that equate a particle with its antiparticle. They harbor diverse potential applications ranging from topological quantum computing [4–10] and topological order [11] to supersymmetry (SUSY) [12–16], quantum chaos, and holographic blackholes [17,18]. In condensed matter, they invariably appear as topologically protected zero energy bound states in topological defects such as superconductor vortices and domain walls [2,3,5–7,10,19–31]. In recent years, the discovery of MMs in Fe-based superconductors with tunable band topology [22,32–44] and the observation of superconductivity in several topological semimetals [45–69] have motivated an urgent quest to theoretically determine the vortex spectrum given an arbitrary normal metal.

This pursuit hits a roadblock with gapless topological matter such as Weyl semimetals (WSMs) [70–88]. In the bulk, WSMs host accidental band crossings or Weyl nodes (WNs) that enjoy topological protection and spawn various topological responses [89–108]. WNs carry an intrinsic chirality or handedness, and are constrained to appear in pairs of opposite chirality [100]. Moreover, in time-reversal ($\mathcal{T}$) symmetric WSMs (TWSMs), each WN has a Kramer's partner of the same chirality which leads to quadruplets of WNs. The surface of a WSM hosts Fermi arcs (FAs) that connect the surface projections of pairs of WNs of opposite chirality [77–86,109–127], resembling a broken segment of a 2D Fermi surface but forming a closed loop with a FA on the opposite surface of a finite slab. The penetration depth of a FA into the bulk depends strongly on the surface momentum and diverges at the WN projections, thus making the surface inseparable from the bulk. Consequently, the Fermi "surface" of WSMs consists of FAs on the surface of the material and bulk Fermi points at the WNs (or Fermi pockets around WNs not at the Fermi level). Such a Fermiology is beyond a purely surface or purely bulk theory; yet, a basic physical question remains, What is the spectrum of a superconductor vortex in a WSM?

General vortex spectrum.—We answer this question using a powerful semiclassical approach that surmounts that above limitation. We restrict to TWSMs, since they generically host a weak pairing instability towards a gapped superconductor; WSMs that lack $\mathcal{T}$ either lack a pairing instability or yield unconventional nodal or finite-momentum pairing [128–131]. For arbitrary pairing symmetry that yields a full gap when uniform, we propose the spectrum

$$E_n^{\pm} = \pm\varepsilon\left(n + \frac{1}{2} + \frac{\Phi_B + \Phi_S - \Phi_Q}{2\pi}\right); \qquad \varepsilon = \frac{\Delta_0}{\xi l_{\mathrm{FA}}} \tag{1}$$

where l_{FA} is of order the total length of FAs on opposite surfaces that form a closed loop, Δ_0 is the pairing amplitude far from the vortex, ξ is the superconductor coherence length, and $n \in \mathbb{Z}$. Additionally, Φ_B is the net phase acquired by a wave packet traversing the bulk. In the simplest case where FAs on opposite surfaces connect the same pairs of WNs as depicted in Fig. 1, $\Phi_B = \Delta\boldsymbol{K}\cdot\boldsymbol{R}_v$ with $\Delta\boldsymbol{K}$ connecting these nodes in momentum space and $\boldsymbol{R}_v$ connecting opposite ends of the vortex in real space. Henceforth, we parameterize $\boldsymbol{R}_v = (a_x\hat{\mathbf{x}} + a_y\hat{\mathbf{y}} + \hat{\mathbf{z}})L_z \equiv (\boldsymbol{a}_\perp + \hat{\mathbf{z}})L_z$, where L_z is the slab thickness and $\hat{\mathbf{z}}$ is the surface normal. Next, Φ_S is the total Berry phase of a "classical" path defined by the FAs on both surfaces that

ignores their bulk penetration. Finally, the penetration effectively reduces the thickness to $L_z - 2d$, where d is the average penetration depth of the FAs in a region of size $O(\xi^{-1})$ around the surface projections of the Weyl nodes. This induces a quantum correction

$$\Phi_Q = 2d\Delta\boldsymbol{K}_\perp \cdot \boldsymbol{a}_\perp \tag{2}$$

where $\Delta\boldsymbol{K}_\perp = \Delta K_x\hat{\mathbf{x}} + \Delta K_y\hat{\mathbf{y}}$. Thus, Eq. (1) predicts a generically nondegenerate, discrete spectrum with equally spaced energy levels, while the zero-point energy is determined by the Berry phase of the FAs, WN locations, sample thickness, and vortex orientation. The spectrum is generically gapped, contrary to a naive bulk approach that predicts a generically gapless spectrum [132].

Equation (1) is inspired by results in Refs. [19,133], and [132]. Reference [133] showed that quasiparticle dynamics in inhomogeneous superconductors can be faithfully captured by quantizing the semiclassical action for wave packets traveling in closed orbits in real space. The action, which appears as a phase in the relevant path integral, was shown to consist of three terms: (i) a Bohr-Sommerfeld phase $\oint \mathbf{k}_{\rm cl} \cdot d\mathbf{r}_{\rm cl}$ for the classical orbit, (ii) a Berry phase due to rotation of the Nambu spinor, and (iii) a π phase if a unit vortex is encircled. Within a complementary momentum-space picture, Ref. [19] proved that a smooth 2D Fermi surface in the normal state and arbitrary pairing symmetry that produces a full gap when superconductivity is uniform yield a superconductor vortex spectrum $\epsilon_n^{\pm} = \pm(\Delta_0/\xi l_{\rm FS})[n + \frac{1}{2} + (\Phi_{\rm FS}/2\pi)]$ for $l_{\rm FS}\xi \gg 1$, where $l_{\rm FS}$ and $\Phi_{\rm FS}$ are the Fermi surface perimeter and Berry phase, respectively. The normal state is assumed to be $\mathcal{T}$ symmetric, which leads to a pair of Fermi surfaces with opposite Berry phases in the normal state that produce particle-hole conjugate eigenstates inside the vortex.

To propose Eq. (1) for a TWSM, we first note that the Bohr-Sommerfeld phase, π phase from the vortex, and the Nambu-Berry phase contribute shifts proportional to n, $1/2$, and $\Phi_{\rm FS}/2\pi$, respectively in ϵ_n. Then, we recall that a WN with chirality $\chi = \pm 1$ produces a chiral MM in the vortex core with chirality χw, where $w = \pm 1$ is the winding number of the vortex [132]. Thus, for $w = 1$, a right- (left-) handed WN produces a chiral MM inside the vortex with upward (downward) group velocity. For a smooth vortex, defined by $|\Delta\boldsymbol{K}\xi| \gg 1$, these chiral modes allow wave packets to travel between FAs on opposite surfaces without scattering. The smoothness also ensures that a wave packet on the surface travels along a single FA without scattering into other FAs. Thus, the semiclassical orbit naturally involves travel along a FA on the top surface, tunneling through the bulk via a downward chiral MM, FA traversal on the bottom surface followed by tunneling up the bulk via an upward chiral MM. Since a TWSM contains quadruplets of WNs and an even number of FAs on each surface related by $\mathcal{T}$, such orbits appear in $\mathcal{T}$-related pairs but with opposite energies in the vortex to preserve overall particle-hole symmetry. This picture inspires the generalization of $\Phi_{\rm FS}$ to $\Phi_{\rm tot} = \Phi_B + \Phi_S - \Phi_Q$, the total phase acquired by a wave packet traversing a closed orbit in mixed real and momentum space, as depicted in Fig. 1.

A peculiar situation occurs when $\Phi_{\rm tot}/2\pi$ equals a half-integer. Then, Eq. (1) predicts a gapless vortex with a pair of zero modes that can always be decomposed into a pair of MMs in a suitable basis [134]. These MMs are highly nonlocal as they are composed of mixed real- and momentum-space orbits. They are not protected by symmetry; rather, they appear at a series of critical points as $\Phi_{\rm tot}$ is varied. These critical points separate trivial and topological phases of the vortex, which behaves as a 0D superconductor with a $\mathbb{Z}_2$ topological classification [135]. The MMs decouple at criticality by definition and, when probed via

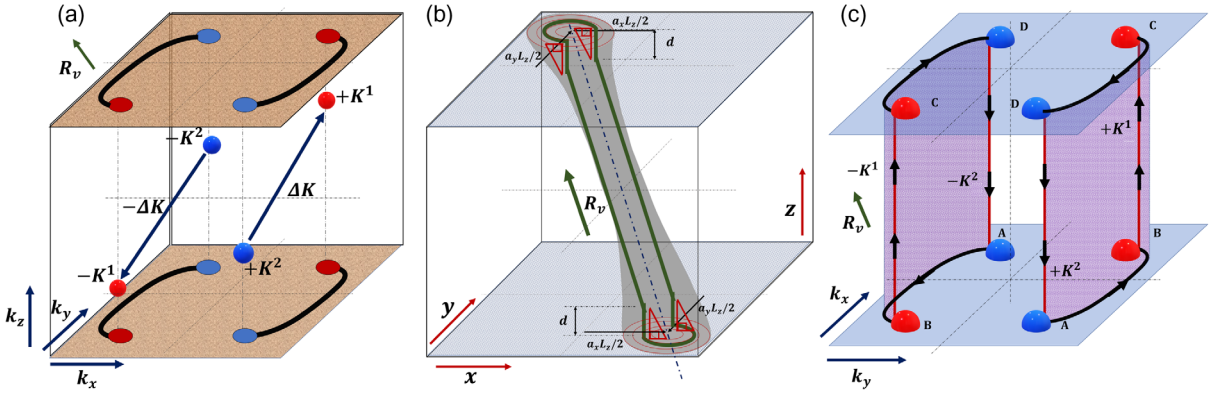

FIG. 1. Schematic picture. (a) $\boldsymbol{k}$-space illustration of a minimal TWSM. Red (blue) spheres at $\pm\boldsymbol{K}^1$ ($\pm\boldsymbol{K}^2$) denote right- (left-)handed WNs, red (blue) discs denote their projections onto the surface Brillouin zone, and black curves are FAs. (b) Real space illustration of the vortex (grey tube) and the semiclassical orbit (green curve). The classical bulk path parallels the tube axis, but quantum tunneling causes deviations near the surface. (c) Semiclassical orbits in mixed real (z) and momentum (k_x, k_y) space. Each orbit is a closed loop consisting of bulk chiral modes tied to a pair of WNs interspersed by FAs that connect their surface projections.

an STM whose tip metal has doubly degenerate bands, contribute separately to the tunneling conductance. Thus, the peak height in the dI/dV spectrum must be twice that of topological MMs [136,137], $2 \times 2e^2/h = 4e^2/h$, while the regions between critical tilts must contain quantized plateaus separated by $4e^2/h$ in the I-V characteristics.

Now, pairs of MMs separate gapped superconductors differing in fermion parity [138]. Thus, the vortex is fermionic with odd fermion parity on the topological side of criticality, and bosonic on the trivial. Naturally, the critical vortex is impartial to bosonic or fermionic statistics and therefore exhibits SUSY—a mysterious and elusive symmetry between bosons and fermions first proposed in the standard model and more recently, in certain condensed matter systems [12–16,139,140] (see Ref. [134] for details). Remarkably, vortices here can be tuned between bosonic, fermionic, and supersymmetric by varying Φ_{tot} which, we show below, can be accomplished by simply tilting the magnetic field that threads the vortex. While disorder, the Zeeman effect and other perturbations can modify the critical tilt angles, SUSY will persist at criticality as it is purely a property of the critical vortex and oblivious to how criticality was achieved.

In general, the vortex also contains purely bulk states that do not involve the FAs. First, WNs at the Fermi level will produce modes $E^{\pm}_{\text{bulk}}(n_1, n_2, q_3) = \pm\sqrt{2\hbar(v_1 n_1 + v_2 n_2)\Delta_0/\xi + (v_3 \hbar q_3)^2}$, where $n_{1,2} \in \mathbb{Z} \geq 0$, $n_1 + n_2 \geq 1$, q_3 is the momentum along the vortex axis measured relative to the WN and (v_1, v_2, v_3) are the canonical Weyl speeds. These modes are nonchiral and lie above the bulk gap $E_g = \sqrt{2\hbar v \Delta_0/\xi}$, where $v = \min(v_{1,2})$. Clearly, $E_g \gg \varepsilon$ if $l_{\text{FA}}\xi \gg \sqrt{\Delta_0 \xi/\hbar v} \sim 1$, assuming the standard Ginzburg-Landau relation $\Delta_0 \sim \hbar v/\xi$. Since $l_{\text{FA}} \sim |\Delta \boldsymbol{K}_\perp| \leq |\Delta \boldsymbol{K}|$, the smooth vortex limit of $|\Delta \boldsymbol{K} \xi| \gg 1$ is consistent with nonchiral bulk modes from undoped WNs being at parametrically higher energies.

Second, the bulk can also contain Fermi pockets. In the weak-pairing, smooth vortex limit, these pockets give rise to the spectrum $E^{\pm}_{\text{bulk}}(n, q_3) = \pm[\Delta_0/\xi l_{\text{FS}}(q_3)]\{n + \frac{1}{2} + [\Phi_{\text{FS}}(q_3)/\Phi_{\text{FS}}(q_3)]\}$ with $n \in \mathbb{Z} \geq 0$. Trivial Fermi pockets that do not enclose band crossings have $\Phi_{\text{FS}}(q_3) \neq \pm\pi \ \forall \ q_3$ and contribute only nonchiral modes. In contrast, Fermi surfaces enclosing WNs have $\Phi_{\text{FS}} = -\pi$ at $q_3 = 0$ (relative to the WN) and contribute a single $n = 0$ chiral MM that combines with the FAs to form the states described in Eq. (1), while the $n \neq 0$ modes are nonchiral. For both types of Fermi pockets, the energy scale of the nonchiral modes $[\Delta_0/\xi l_{\text{FS}}(q_z)] \lesssim \varepsilon$ if $l_{\text{FS}} \gtrsim l_{\text{FA}}$. However, these modes can be easily distinguished from those defined in Eq. (1) by tilting the vortex, as we discuss shortly.

Finally, the normal state bulk can contain other point or line band crossings too which can invalidate various aspects of our results. For instance, vortices in Dirac semimetals contain a pair of counterpropagating modes for each Dirac node [141–143], which can hybridize and ruin the semiclassical picture. We ignore crossings beyond unit WNs because they rely on crystalline symmetries while our focus is on generic band structures with only $\mathcal{T}$ symmetry [144–146].

Numerical vortex spectrum.—We now support our general claims of Eq. (1) with numerics on an orthorhombic lattice model of a TWSM detailed in [134]. Given the Bloch Hamiltonian $H_0(\boldsymbol{k}, k_z)$ in the normal state, the corresponding Bogoliubov-deGennes Hamiltonian for a unit vortex along $(a_x, a_y, 1)$ can be written as

$$H_v = \begin{pmatrix} H_0(\boldsymbol{k}, k_z) & \Delta(\delta \boldsymbol{r}_\perp) e^{-i\Theta(\delta \mathbf{r}_\perp)} \\ \Delta(\delta \boldsymbol{r}_\perp) e^{i\Theta(\delta \mathbf{r}_\perp)} & -H_0(\boldsymbol{k}, k_z) \end{pmatrix} \tag{3}$$

where $\delta \boldsymbol{r}_\perp = (x - a_x z, y - a_y z)$, $\Theta(\delta \boldsymbol{r}_\perp)$ is the polar angle of $\delta \boldsymbol{r}_\perp$ and $\Delta(\delta \boldsymbol{r}_\perp) = \Delta_0 \tanh(|\delta \boldsymbol{r}_\perp|/\xi)$. Direct numerical verification of Eq. (1) involves diagonalizing H_v in real space. However, the lack of translation invariance in every direction limits us to relatively small ξ, which causes departure from semiclassics for modest values of n. We bypass this limitation by tilting the vortex and comparing the locations of the zero modes with the predictions of Eq. (1). This way, we always probe the lowest few energy levels, which conform better to the semiclassical analysis. While this method allows a careful examination of the Berry phase terms and reveals various striking phenomena, ε is verifiable only up to its order of magnitude.

Figure 2(a) shows the FAs and WNs in a minimal TWSM with four WNs located at $\pm\boldsymbol{K}^1$ and $\pm\boldsymbol{K}^2$. We chose parameters such that all nodes are at different k_z and $|\Delta K_x| \ll |\Delta K_y|$ where $\Delta \boldsymbol{K} = \boldsymbol{K}^1 - \boldsymbol{K}^2$. Figure 2(b) shows the vortex spectrum for a finite slab when a vortex, initially along $\hat{\mathbf{z}}$, is tilted separately towards the x and the y axis. Tilting towards the positive y axis ($a_x = 0$, $a_y > 0$) produces numerous level crossings, which is consistent with $\Phi_B = (\Delta K_y a_y + \Delta K_z) L_z$ changing by many multiples of 2π as a_y varies. In contrast, the spectrum varies weakly when the vortex is tilted towards the x axis, which is consistent with $\Phi_B = \Delta K_x a_x L_z$ varying negligibly with a_x since ΔK_x itself is small. In Fig. 2(c), we plot the wave functions of a pair of levels with equal and opposite energies in (k_x, k_y, z) space. The levels, which are related by particle-hole symmetry of the superconductor, are clearly localized around semiclassical orbits related by $\mathcal{T}$. This confirms the picture that motivated Eq. (1), namely, that the vortex spectrum follows from quantizing semiclassical orbits in mixed real and momentum space, and that semiclassical orbits related by $\mathcal{T}$ turn into pairs of particle-hole conjugate quantum eigenstates. In [134], we use the zero mode locations to extract $\Delta K_{y,z}$ and Φ_S and find remarkable agreement with expectations.

Tilting the vortex.—Besides simplifying the numerics, tilting the vortex leads to striking qualitative phenomena.

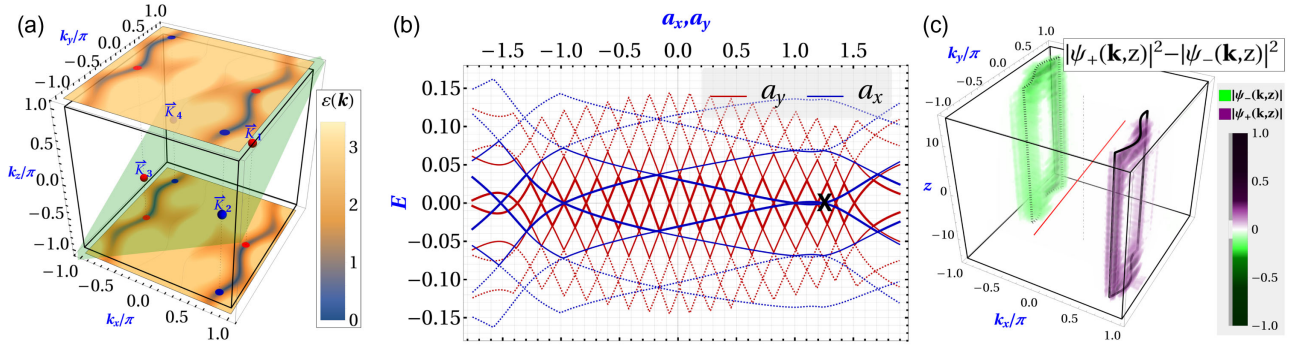

FIG. 2. Vortex spectrum for a tight-binding lattice model with unit interatomic spacing and $O(1)$ hoppings (see Ref. [134] for details). (a) Normal state band structure showing four bulk WNs (red and blue spheres), all at different k_z, and surface FAs connecting them. The four nodes lie on the green plane, which is clearly not parallel to the surface. (b) Vortex spectrum of a $L_x \times L_y \times L_z = 23 \times 23 \times 34$ system as the vortex is tilted separately towards the x axis and the y axis by $\tan^{-1} a_i$ $(i = x, y)$. (c) Net probability density of the two lowest energy wave functions in (k_x, k_y, z) space at $a_y = 1.25$, marked "X" in (b), obtained by Fourier transforming the 3D real space wave functions with respect to x, y. We choose the band parameter $u = 1.2$ which yields $\Delta \boldsymbol{K}^{\text{calc}} = \{0.029, 0.428, 0.181\} \times 2\pi$, and superconducting parameters $\Delta_0 = 0.50$, $\xi = 2.0$, which yield $\varepsilon = \Delta_0/\xi l_{\text{FA}} \approx 0.04$ comparable to the scale of level spacings in (b).

First, since L_z enters Eq. (1) only through Φ_B, the spectrum becomes L_z independent when the vortex is tilted to a "magic angle" such that $\Delta \boldsymbol{K} \perp \boldsymbol{R}_v$ even though the semiclassical orbit still involves travel across the bulk. Moreover, we expect peaks in the density of states, $D(E) = \sum_{n,\lambda} \delta(E - E_n^{\lambda})$, whenever $E_n^{\pm} = 0$. Noting that Φ_S does not depend on the vortex orientation, $D(0)$ peaks whenever $\Delta \boldsymbol{K}_\perp \cdot \boldsymbol{a}_\perp (L_z - 2d)$ equals a half-integer. Thus, the tilt parameters for two successive peaks obey

$$\Delta \boldsymbol{K}_\perp \cdot [\boldsymbol{a}_\perp^{(j)} - \boldsymbol{a}_\perp^{(j+1)}] = \frac{2\pi}{L_z - 2d}. \tag{4}$$

Thus, the peaks are periodic in $\boldsymbol{a}_\perp$ with a period Δa governed by the WN locations through $\Delta \boldsymbol{K}_\perp$ and the effective thickness, $L_z - 2d$. Specifically, $\Delta a = [2\pi/(L_z - 2d)\Delta K_t]$, where ΔK_t is the component of $\Delta \boldsymbol{K}_\perp$ in the tilt direction.

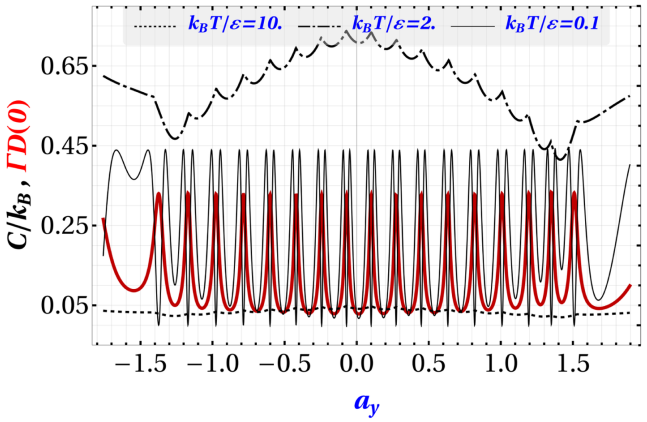

FIG. 3. Suitably normalized density of states $D(0)$ and specific heat C at different temperatures versus a_y. Zero modes in the spectrum lead to sharp peaks in $D(0)$ at periodic intervals of a_y, $\Delta a_y = [2\pi/(L_z - 2d)\Delta K_y]$, and induce oscillations in C at low T that get smeared out at high T. We approximate $D(E) = \pi^{-1} \text{Im} \sum_n [E - E_n - i\Gamma]^{-1}$ with $\Gamma = 0.0075$.

These peaks will induce characteristic oscillations with period Δa in transport and thermodynamic quantities at temperatures below the minigap, $T \lesssim \varepsilon/k_B$. For instance, the specific heat $C = k_B \sum_n [(E_n^+/k_BT)\text{sech}(E_n^+/k_BT)]^2$ will have oscillations with a "split-peak" structure (Fig. 3). Similarly, a scanning tunneling microscope (STM) should find zero bias peaks in the differential conductance, dI/dV, at periodic tilts with a peak height of $4e^2/h$. These oscillations can be used to distinguish the semiclassical modes depicted in Fig. 1 from nonchiral vortex modes generated by bulk Fermi pockets. The latter are expected to produce only quantitative variations due to the anisotropy of the Fermi pockets, but no oscillations or L_z dependence besides finite-size effects.

The magic angle and oscillations are reminiscent of quantum oscillations due to FAs in WSMs [126,127,147]. There, a magnetic field B induces cyclotron orbits involving surface FAs and bulk chiral modes, $D(0)$ has periodic peaks in $1/B$, and L_z enters the oscillation phase as an optical path length. Thus, at the quantum level, the discretization predicted by Eq. (1) is analogous to Landau levels rather than finite size quantization. Indeed, if the latter was at play, Eq. (1) in the thermodynamic limit should have yielded the gapless bulk spectrum described in Ref. [132] where FAs are irrelevant. It clearly does not, which can be attributed to the infinite penetration of the FAs into the bulk that forbids ignoring them even in this limit.

Application to (Nb,Ta)P.—NbP and TaP are TWSMs in which superconductivity induced at high pressure survives upon quenching to ambient pressure [51,62]. Superconductivity has also been reported in TaP directly at ambient pressure [69]. Both materials have 24 Weyl nodes interrelated by C_4 symmetry of a face-centered tetragonal lattice with conventional unit cell lattice constants $a_{\text{NbP}} = 0.3334\,\text{nm}$, $c_{\text{NbP}} = 1.1376\,\text{nm}$ and $a_{\text{TaP}} = 0.3318\,\text{nm}$, $c_{\text{TaP}} = 1.1363\,\text{nm}$ [148], and connected by 12 pairs of surface FAs. Although nonuniversal surface details

strongly modify the FAs and lead to nontopological gapless surface states from trivial Fermi surfaces [83,149], a smooth superconductor vortex tilted in a general direction is expected to produce 12 pairs of $\mathcal{T}$-related semiclassical orbits and hence, a superposition of 12 different oscillations frequencies in dI/dV. On the other hand, tilting in the yz plane ensures that only orbits with nonzero ΔK_y cause oscillations. If FAs connect surface projections of the nearest nodes of the same family, then $\Delta K_y = 0$ for all six orbits that involve WNs separated by the yz plane, while C_4^2 and $\mathcal{T}$ symmetries ensure that the six orbits that cross the xz plane will result in precisely two frequencies: one from WNs with $\Delta \boldsymbol{K}^1_{\perp,\mathrm{NbP}} = 1.0198 \times (2\pi/a_{\mathrm{NbP}})\hat{\mathbf{y}}$ for NbP and $\Delta \boldsymbol{K}^1_{\perp,\mathrm{TaP}} = 0.9618 \times (2\pi/a_{\mathrm{TaP}})\hat{\mathbf{y}}$ for TaP, and another from WNs with $\Delta \boldsymbol{K}^2_{\perp,\mathrm{NbP}} = 0.5406 \times (2\pi/c_{\mathrm{NbP}})\hat{\mathbf{y}}$ and $\Delta \boldsymbol{K}^2_{\perp,\mathrm{TaP}} = 0.5486 \times (2\pi/c_{\mathrm{TaP}})\hat{\mathbf{y}}$. Discernible oscillations require $T \lesssim \varepsilon/k_B = \Delta_0/\xi l_{\mathrm{FA}} k_B \sim T_c/\xi l_{\mathrm{FA}}$. Using $T_c \sim 4$ K [51,62], $\xi \sim 4$ nm [58] and $l_{\mathrm{FA}} \sim 10\ \mathrm{nm}^{-1}$ gives $T \lesssim 0.1$ K, which may be within reach of current STM experiments. Note that ε is of the same order as the vortex minigap in typical type-II superconductors, and STM can comfortably probe vortex modes in the latter including zero bias conductance peaks from MMs [22,33–38,150].

In summary, we have calculated the superconductor vortex spectrum in TWSMs including contributions from the surface FAs. While a naive bulk calculation for a general vortex orientation suggests a gapless spectrum consisting of a chiral mode corresponding to each WN, we found that the low-energy spectrum is gapped in general, and determined by the Berry phase of semiclassical orbits composed of the chiral modes and surface FAs. Such a spectrum is expected to produce a myriad of striking phenomena upon tilting the vortex. For instance, the vortex will alternate between bosonic and fermionic as it is tilted, while the critical points separating the two types of vortices exhibit SUSY and harbor unusual nonlocal MMs. Experimentally, we predict characteristic oscillations in the specific heat and periodic, $4e^2/h$-quantized peaks in the differential tunneling conductance as a function of vortex tilt. At a certain tilt, dubbed the "magic angle," the spectrum becomes independent of the slab thickness. We propose NbP and TaP as candidate materials and tunneling spectroscopy as the best experimental approach for studying this physics.

We thank Liangzi Deng, Laura Greene, Kun Yang, Elio Koenig, Urjit Yajnik, Ashvin Vishwanath, and Binghai Yan for valuable discussions and comments, and acknowledge financial support from the National Science Foundation under Grant No. DMR-2047193.

[1] C. Caroli, P. G. De Gennes, J. Matricon, P. G. De Gennes, and J. Matricon, Bound fermion states on a vortex line in a type II superconductor, Phys. Lett. **9**, 307 (1964).

[2] N. Read and Dmitry Green, Paired states of fermions in two dimensions with breaking of parity and time-reversal symmetries and the fractional quantum Hall effect, Phys. Rev. B **61**, 10267 (2000).

[3] Liang Fu and C. L. Kane, Superconducting Proximity Effect and Majorana Fermions at the Surface of a Topological Insulator, Phys. Rev. Lett. **100**, 096407 (2008).

[4] A. Yu. Kitaev, Fault-tolerant quantum computation by anyons, Ann. Phys. (Amsterdam) **303**, 2 (2003).

[5] Jason Alicea, New directions in the pursuit of Majorana fermions in solid state systems, Rep. Prog. Phys. **75**, 076501 (2012).

[6] C. W. J. Beenakker, Search for Majorana fermions in superconductors, Annu. Rev. Condens. Matter Phys. **4**, 113 (2013).

[7] Steven R. Elliott and Marcel Franz, Colloquium: Majorana fermions in nuclear, particle, and solid-state physics, Rev. Mod. Phys. **87**, 137 (2015).

[8] Leo Kouwenhoven, Majorana qubits, *Technical Digest—International Electron Devices Meeting, IEDM* (IEEE, San Francisco, CA, 2019).

[9] R. M. Lutchyn, E. P. A. M. Bakkers, L. P. Kouwenhoven, P. Krogstrup, C. M. Marcus, and Y. Oreg, Majorana zero modes in superconductor–semiconductor heterostructures, Nat. Rev. Mater. **3**, 52 (2018).

[10] Ning Ma, Majorana fermions in condensed matter: An outlook, Physica (Amsterdam) **512B**, 100 (2017).

[11] Alexei Kitaev, Anyons in an exactly solved model and beyond, Ann. Phys. (Amsterdam) **321**, 2 (2006), January Special Issue.

[12] Tarun Grover and Ashvin Vishwanath, Quantum criticality in topological insulators and superconductors: Emergence of strongly coupled majoranas and supersymmetry, arXiv:1206.1332.

[13] Tarun Grover, D. N. Sheng, and Ashvin Vishwanath, Emergent space-time supersymmetry at the boundary of a topological phase, Science **344**, 280 (2014).

[14] Armin Rahmani, Xiaoyu Zhu, Marcel Franz, and Ian Affleck, Emergent Supersymmetry from Strongly Interacting Majorana Zero Modes, Phys. Rev. Lett. **115**, 166401 (2015).

[15] Timothy H. Hsieh, Gábor B. Halász, and Tarun Grover, All Majorana Models with Translation Symmetry are Supersymmetric, Phys. Rev. Lett. **117**, 166802 (2016).

[16] Zhao Huang, Shinji Shimasaki, and Muneto Nitta, Supersymmetry in closed chains of coupled majorana modes, Phys. Rev. B **96**, 220504(R) (2017).

[17] Juan Maldacena and Douglas Stanford, Remarks on the Sachdev-Ye-Kitaev model, Phys. Rev. D **94**, 106002 (2016).

[18] A Kitaev, A simple model of quantum holography, https://online.kitp.ucsb.edu/online/entangled15/kitaev/.

[19] P. Hosur, P. Ghaemi, R. S. K. Mong, and A. Vishwanath, Majorana Modes at the Ends of Superconductor Vortices in Doped Topological Insulators, Phys. Rev. Lett. **107**, 097001 (2011).

[20] A. Yu. Kitaev, Unpaired Majorana fermions in quantum wires, Phys. Usp. **44**, 131 (2001).

[21] Martin Leijnse and Karsten Flensberg, Introduction to topological superconductivity and Majorana fermions, Semicond. Sci. Technol. **27**, 124003 (2012).

[22] Qin Liu, Chen Chen, Tong Zhang, Rui Peng, Ya Jun Yan, Chen Hao Ping Wen, Xia Lou, Yu Long Huang, Jin Peng Tian, Xiao Li Dong, Guang Wei Wang, Wei Cheng Bao, Qiang Hua Wang, Zhi Ping Yin, Zhong Xian Zhao, and Dong Lai Feng, Robust and Clean Majorana Zero Mode in the Vortex Core of High-Temperature Superconductor (Li0.84Fe0.16)OHFeSe, Phys. Rev. X **8**, 041056 (2018).

[23] Xiao Ping Liu, Yuan Zhou, Yi Fei Wang, and Chang De Gong, Characterizations of topological superconductors: Chern numbers, edge states and Majorana zero modes, New J. Phys. **19**, 093018 (2017).

[24] Roman M. Lutchyn, Tudor D. Stanescu, and S. Das Sarma, Search for Majorana Fermions in Multiband Semiconducting Nanowires, Phys. Rev. Lett. **106**, 127001 (2011).

[25] N. Mohanta and A. Taraphder, Topological superconductivity and Majorana bound states at the LaAlO3/SrTiO3 interface, Europhys. Lett. **108** (2014).

[26] V. Mourik, K. Zuo, S. M. Frolov, S. R. Plissard, E. P. A. M. Bakkers, and L. P. Kouwenhoven, Signatures of Majorana fermions in hybrid superconductor-semiconductor nanowire devices, Science **336**, 1003 (2012).

[27] Stevan Nadj-Perge, Ilya K. Drozdov, Jian Li, Hua Chen, Sangjun Jeon, Jungpil Seo, Allan H. MacDonald, B. Andrei Bernevig, and Ali Yazdani, Observation of Majorana fermions in ferromagnetic atomic chains on a superconductor, Science **346**, 602 (2014).

[28] Xiao-Liang Qi and Shou-Cheng Zhang, Topological insulators and superconductors, Rev. Mod. Phys. **83**, 1057 (2011).

[29] Leonid P. Rokhinson, Xinyu Liu, and Jacek K. Furdyna, The fractional a.c. Josephson effect in a semiconductor–superconductor nanowire as a signature of Majorana particles, Nat. Phys. **8**, 795 (2012).

[30] Masatoshi Sato and Satoshi Fujimoto, Existence of Majorana Fermions and Topological Order in Nodal Superconductors with Spin-Orbit Interactions in External Magnetic Fields, Phys. Rev. Lett. **105**, 217001 (2010).

[31] Masatoshi Sato and Yoichi Ando, Topological superconductors: A review, Rep. Prog. Phys. **80**, 076501 (2017).

[32] Peng Zhang *et al.*, Observation of topological superconductivity on the surface of an iron-based superconductor, Science **360**, 182 (2018).

[33] Lingyuan Kong, Shiyu Zhu, Hui Papaj Michaland Chen, Lu Cao, Hiroki Isobe, Yuqing Xing, Wenyao Liu, Dongfei Wang, Peng Fan, Yujie Sun, Shixuan Du, John Schneeloch, Ruidan Zhong, Genda Gu, Liang Fu, Hong-Jun Gao, and Hong Ding, Half-integer level shift of vortex bound states in an iron-based superconductor, Nat. Phys. **15**, 1181 (2019).

[34] Shiyu Zhu, Lingyuan Kong, Lu Cao, Hui Chen, Michał Papaj, Shixuan Du, Yuqing Xing, Wenyao Liu, Dongfei Wang, Chengmin Shen, Fazhi Yang, John Schneeloch, Ruidan Zhong, Genda Gu, Liang Fu, Yu-Yang Zhang, Hong Ding, and Hong-Jun Gao, Nearly quantized conductance plateau of vortex zero mode in an iron-based superconductor, Science **367**, 189 (2020).

[35] Dongfei Wang, Lingyuan Kong, Peng Fan, Hui Chen, Shiyu Zhu, Wenyao Liu, Lu Cao, Yujie Sun, Shixuan Du, John Schneeloch, Ruidan Zhong, Genda Gu, Liang Fu, Hong Ding, and Hong-Jun Gao, Evidence for Majorana bound states in an iron-based superconductor, Science **362**, 333 (2018).

[36] T. Machida, Y. Sun, S. Pyon, S. Takeda, Y. Kohsaka, T. Hanaguri, T. Sasagawa, and T. Tamegai, Zero-energy vortex bound state in the superconducting topological surface state of Fe(Se,Te), Nat. Mater. **18**, 811 (2019).

[37] Wenyao Liu, Lu Cao, Shiyu Zhu, Lingyuan Kong, Guangwei Wang, Michał Papaj, Peng Zhang, Ya-Bin Liu, Hui Chen, Geng Li, Fazhi Yang, Takeshi Kondo, Shixuan Du, Guang-Han Cao, Shik Shin, Liang Fu, Zhiping Yin, Hong-Jun Gao, and Hong Ding, A new Majorana platform in an fe-as bilayer superconductor, Nat. Commun. **11**, 5688 (2020).

[38] Lingyuan Kong, Lu Cao, Shiyu Zhu, Michał Papaj, Guangyang Dai, Geng Li, Peng Fan, Wenyao Liu, Fazhi Yang, Xiancheng Wang, Shixuan Du, Changqing Jin, Liang Fu, Hong-Jun Gao, and Hong Ding, Majorana zero modes in impurity-assisted vortex of lifeas superconductor, Nat. Commun. **12**, 4146 (2021).

[39] Zhijun Wang, P. Zhang, Gang Xu, L. K. Zeng, H. Miao, Xiaoyan Xu, T. Qian, Hongming Weng, P. Richard, A. V. Fedorov, H. Ding, Xi Dai, and Zhong Fang, Topological nature of the $fese_{0.5}te_{0.5}$ superconductor, Phys. Rev. B **92**, 115119 (2015).

[40] X.-L. Peng, Y. Li, X.-X. Wu, H.-B. Deng, X. Shi, W.-H. Fan, M. Li, Y.-B. Huang, T. Qian, P. Richard, J.-P. Hu, S.-H. Pan, H.-Q. Mao, Y.-J. Sun, and H. Ding, Observation of topological transition in high-T_c superconducting monolayer $fete_{1-x}se_x$ films on $srtio_3(001)$, Phys. Rev. B **100**, 155134 (2019).

[41] Gang Xu, Biao Lian, Peizhe Tang, Xiao-Liang Qi, and Shou-Cheng Zhang, Topological Superconductivity on the Surface of Fe-Based Superconductors, Phys. Rev. Lett. **117**, 047001 (2016).

[42] Peng Zhang *et al.*, Multiple topological states in iron-based superconductors, Nat. Phys. **15**, 41 (2019).

[43] Shengshan Qin, Lunhui Hu, Xianxin Wu, Xia Dai, Chen Fang, Fu-Chun Zhang, and Jiangping Hu, Topological vortex phase transitions in iron-based superconductors, Sci. Bull. **64**, 1207 (2019).

[44] Areg Ghazaryan, Pedro L. S. Lopes, Pavan Hosur, Matthew J. Gilbert, and Pouyan Ghaemi, Effect of Zeeman coupling on the Majorana vortex modes in iron-based topological superconductors, Phys. Rev. B **101**, 020504 (2020).

[45] Leena Aggarwal, Abhishek Gaurav, Gohil S. Thakur, Zeba Haque, Ashok K. Ganguli, and Goutam Sheet, Unconventional superconductivity at mesoscopic point contacts on the 3D Dirac semimetal Cd3As2, Nat. Mater. **15**, 32 (2015).

[46] Leena Aggarwal, Sirshendu Gayen, Shekhar Das, Ritesh Kumar, Vicky Süß, Claudia Felser, Chandra Shekhar, and Goutam Sheet, Mesoscopic superconductivity and high spin polarization coexisting at metallic point contacts on Weyl semimetal TaAs, Nat. Commun. **8**, 13974 (2017).

[47] M. Alidoust, K. Halterman, and A. A. Zyuzin, Superconductivity in type-II Weyl semimetals, Phys. Rev. B **95**, 155124 (2017).

[48] Maja D. Bachmann, Nityan Nair, Felix Flicker, Roni Ilan, Tobias Meng, Nirmal J. Ghimire, Eric D. Bauer, Filip

Ronning, James G. Analytis, and Philip J. W. Moll, Inducing superconductivity in Weyl semimetal microstructures by selective ion sputtering, Sci. Adv. **3**, 1 (2017).

[49] Shu Cai, Eve Emmanouilidou, Jing Guo, Xiaodong Li, Yanchun Li, Ke Yang, Aiguo Li, Qi Wu, Ni Ni, and Liling Sun, Observation of superconductivity in the pressurized Weyl-semimetal candidate TaIrTe4, Phys. Rev. B **99**, 020503 (2019).

[50] F. C. Chen, X. Luo, R. C. Xiao, W. J. Lu, B. Zhang, H. X. Yang, J. Q. Li, Q. L. Pei, D. F. Shao, R. R. Zhang, L. S. Ling, C. Y. Xi, W. H. Song, and Y. P. Sun, Superconductivity enhancement in the S-doped Weyl semimetal candidate MoTe2, Appl. Phys. Lett. **108**, 162601 (2016).

[51] Wen Deng, Jiapeng Zhen, Qiushi Huang, Yanju Wang, Hongliang Dong, Shun Wan, Shihui Zhang, Jiajia Feng, and Bin Chen, Pressure-quenched superconductivity in Weyl semimetal NBP induced by electronic phase transitions under pressure, J. Phys. Chem. Lett. **13**, 5514 (2022).

[52] Sirshendu Gayen, Leena Aggarwal, and Goutam Sheet, Comment on "Tip induced unconventional superconductivity on Weyl semimetal TaAs", Sci. Bull. **62**, 425 (2017).

[53] Z. Guguchia *et al.*, Signatures of the topological s +− superconducting order parameter in the type-II Weyl semimetal T d-MoTe2, Nat. Commun. **8**, 1 (2017).

[54] Lanpo He, Yating Jia, Sijia Zhang, Xiaochen Hong, Changqing Jin, and Shiyan Li, Pressure-induced superconductivity in the three-dimensional topological Dirac semimetal Cd3As2, npj Quantum Mater. **1**, 16014 (2016).

[55] Ce Huang *et al.*, Inducing strong superconductivity in WTe2 by a proximity effect, ACS Nano **12**, 7185 (2018).

[56] Ce Huang *et al.*, Proximity-induced surface superconductivity in Dirac semimetal Cd3As2, Nat. Commun. **10**, 2217 (2019).

[57] Defen Kang, Yazhou Zhou, Wei Yi, Chongli Yang, Jing Guo, Youguo Shi, Shan Zhang, Zhe Wang, Chao Zhang, Sheng Jiang, Aiguo Li, Ke Yang, Qi Wu, Guangming Zhang, Liling Sun, and Zhongxian Zhao, Superconductivity emerging from a suppressed large magnetoresistant state in tungsten ditelluride, Nat. Commun. **6**, 7804 (2015).

[58] Yejin Lee, Omkaram Inturu, Jin Hee Kim, and Jong-Soo Rhyee, Robust bulk superconductivity by giant proximity effect in Weyl semimetal-superconducting NbP/$NbSe_2$ composites, 2021, 10.21203/rs.3.rs-890116/v1.

[59] Yufeng Li, Yonghui Zhou, Zhaopeng Guo, Xuliang Chen, Pengchao Lu, Xuefei Wang, Chao An, Ying Zhou, Jie Xing, Guan Du, Xiyu Zhu, Huan Yang, Jian Sun, Zhaorong Yang, Yuheng Zhang, and Hai-Hu Wen, Superconductivity induced by high pressure in Weyl semimetal TaP, npj Quantum Mater. **2**, 66 (2017).

[60] Yanan Li, Qiangqiang Gu, Chen Chen, Jun Zhang, Qin Liu, Xiyao Hu, Jun Liu, Yi Liu, Langsheng Ling, Mingliang Tian, Yong Wang, Nitin Samarth, Shiyan Li, Tong Zhang, Ji Feng, and Jian Wang, Nontrivial superconductivity in topological MoTe(2-x)S(x) crystals, Proc. Natl. Acad. Sci. U.S.A. **115**, 9503 (2018).

[61] Yupeng Li, Chao An, Chenqiang Hua, Xuliang Chen, Ying Yonghui Zhou, Ying Yonghui Zhou, Ranran Zhang, Changyong Park, Zhen Wang, Yunhao Lu, Yi Zheng, Zhaorong Yang, and Zhu-an An Xu, Pressure-induced superconductivity in topological semimetal, npj Quantum Mater. **3** (2018).

[62] Yufeng Li, Yonghui Zhou, Zhaopeng Guo, Fei Han, Xuliang Chen, Pengchao Lu, Xuefei Wang, Chao An, Ying Zhou, Jie Xing, Guan Du, Xiyu Zhu, Huan Yang, Jian Sun, Zhaorong Yang, Wenge Yang, Ho-Kwang Mao, Yuheng Zhang, and Hai-Hu Wen, Concurrence of superconductivity and structure transition in Weyl semimetal TaP under pressure, npj Quantum Mater. **2**, 66 (2017).

[63] Xing-Chen Pan, Xuliang Chen, Huimei Liu, Yanqing Feng, Zhongxia Wei, Yonghui Zhou, Zhenhua Chi, Li Pi, Fei Yen, Fengqi Song, Xiangang Wan, Zhaorong Yang, Baigeng Wang, Guanghou Wang, and Yuheng Zhang, Pressure-driven dome-shaped superconductivity and electronic structural evolution in tungsten ditelluride, Nat. Commun. **6**, 7805 (2015).

[64] Yanpeng Qi *et al.*, Superconductivity in Weyl semimetal candidate MoTe2, Nat. Commun. **7**, 11038 (2016).

[65] O. O. Shvetsov, V. D. Esin, A. V. Timonina, N. N. Kolesnikov, and E. V. Deviatov, Surface superconductivity in a three-dimensional Cd3As2 semimetal at the interface with a gold contact, Phys. Rev. B **99**, 125305 (2019).

[66] Huichao He Wang, Huichao He Wang, Yuqin Chen, Jiawei Luo, Zhujun Yuan, Jun Liu, Yong Wang, Shuang Jia, Xiong-Jun Liu, Jian Wei, and Jian Wang, Discovery of tip induced unconventional superconductivity on Weyl semimetal, Sci. Bull. **62**, 425 (2017).

[67] He Wang, Huichao Wang, Haiwen Liu, Hong Lu, Wuhao Yang, Shuang Jia, Xiong-Jun Liu, X. C. Xie, Jian Wei, and Jian Wang, Observation of superconductivity induced by a point contact on 3D Dirac semimetal Cd3As2 crystals, Nat. Mater. **15**, 38 (2015).

[68] Ying Xing, Zhibin Shao, Jun Ge, Jiawei Luo, Jian Jinhua Wang, Zengwei Zhu, Jun Liu, Yong Wang, Zhiying Zhao, Jiaqiang Yan, David Mandrus, Binghai Yan, Xiong-Jun Liu, Minghu Pan, and Jian Jinhua Wang, Surface superconductivity in the type II Weyl semimetal $TaIrTe_4$, Natl. Sci. Rev. **7**, 579 (2019).

[69] Maarten R. van Delft, Sergio Pezzini, Markus Konig, Paul Tinnemans, Nigel E. Hussey, and Steffen Wiedmann, Two- and three-dimensional superconducting phases in the Weyl semimetal TaP at ambient pressure, Crystals **10**, 288 (2020).

[70] Oskar Vafek and Ashvin Vishwanath, Dirac fermions in solids: From high-Tc cuprates and graphene to topological insulators and Weyl semimetals, Annu. Rev. Condens. Matter Phys. **5**, 83 (2014).

[71] A. A. Burkov, Weyl metals, Annu. Rev. Condens. Matter Phys. **9**, 359 (2018).

[72] A. A. Burkov, Topological semimetals, Nat. Mater. **15**, 1145 (2016).

[73] Binghai Yan and Claudia Felser, Topological materials: Weyl semimetals, Annu. Rev. Condens. Matter Phys. **8**, 337 (2017).

[74] N. P. Armitage, E. J. Mele, and Ashvin Vishwanath, Weyl and Dirac semimetals in three-dimensional solids, Rev. Mod. Phys. **90**, 015001 (2018).

[75] Shun-Qing Shen, Topological insulators, in *Topological Dirac and Weyl Semimetals*, Volume 187 of Springer Series in Solid-State Sciences (Springer, Singapore, 2017), pp. 207–229.

[76] Ilya Belopolski *et al.*, Discovery of a new type of topological Weyl fermion semimetal state in MoxW1-xTe2, Nat. Commun. **7**, 13643 (2016).

[77] Zhao Peng Guo, Peng Chao Lu, Tong Chen, Jue Fei Wu, Jian Sun, and Ding Yu Xing, High-pressure phases of Weyl semimetals NbP, NbAs, TaP, and TaAs, Sci. China Phys. Mech. **61**, 038211 (2018).

[78] Guoqing Chang, Su-Yang Xu, Hao Zheng, Chi-Cheng Lee, Shin-Ming Huang, Ilya Belopolski, Daniel S Sanchez, Guang Bian, Nasser Alidoust, Tay-Rong Chang, Chuang-Han Hsu, Horng-Tay Jeng, Arun Bansil, Hsin Lin, and M Zahid Hasan, Signatures of Fermi Arcs in the Quasiparticle Interferences of the Weyl Semimetals TaAs and NbP, Phys. Rev. Lett. **116**, 066601 (2016).

[79] András Gyenis, Hiroyuki Inoue, Sangjun Jeon, Brian B. Zhou, Benjamin E. Feldman, Zhijun Wang, Jian Li, Shan Jiang, Quinn D. Gibson, Satya K. Kushwaha, Jason W. Krizan, Ni Ni, Robert J. Cava, B. Andrei Bernevig, and Ali Yazdani, Imaging electronic states on topological semimetals using scanning tunneling microscopy, New J. Phys. **18**, 105003 (2016).

[80] Shin-Ming Huang, Su-Yang Xu, Ilya Belopolski, Chi-Cheng Lee, Guoqing Chang, BaoKai Wang, Nasser Alidoust, Guang Bian, Madhab Neupane, Chenglong Zhang, Shuang Jia, Arun Bansil, Hsin Lin, and M. Zahid Hasan, A Weyl Fermion semimetal with surface Fermi arcs in the transition metal monopnictide TaAs class, Nat. Commun. **6**, 7373 (2015).

[81] Hiroyuki Inoue, András Gyenis, Zhijun Wang, Jian Li, Seong Woo Oh, Shan Jiang, Ni Ni, B Andrei Bernevig, and Ali Yazdani, Quasiparticle interference of the Fermi arcs and surface-bulk connectivity of a Weyl semimetal, Science **351**, 1184 (2016).

[82] B. Q. Lv, N. Xu, H. M. Weng, J. Z. Ma, P. Richard, X. C. Huang, L. X. Zhao, G. F. Chen, C. E. Matt, F. Bisti, V. N. Strocov, J. Mesot, Z. Fang, X. Dai, T. Qian, M. Shi, and H. Ding, Observation of Weyl nodes in TaAs, Nat. Phys. **11**, 724 (2015).

[83] Yan Sun, Shu Chun Wu, and Binghai Yan, Topological surface states and Fermi arcs of the noncentrosymmetric Weyl semimetals TaAs, TaP, NbAs, and NbP, Phys. Rev. B **92**, 115428 (2015).

[84] Su-yang Xu *et al.*, Discovery of a Weyl Fermion Semimetal, Science **349**, 613 (2015).

[85] Su Yang Xu *et al.*, Spin Polarization and Texture of the Fermi Arcs in the Weyl Fermion Semimetal TaAs, Phys. Rev. Lett. **116**, 096801 (2016).

[86] Su-Yang Xu *et al.*, Discovery of a Weyl fermion semimetal and topological Fermi arcs, Science **349**, 613 (2015).

[87] L. X. Yang, Z. K. Liu, Y. Sun, H. Peng, H. F. Yang, T. Zhang, B. Zhou, Y. Zhang, Y. F. Guo, M. Rahn, D. Prabhakaran, Z. Hussain, S. K. Mo, C. Felser, B. Yan, and Y. L. Chen, Weyl semimetal phase in the noncentrosymmetric compound TaAs, Nat. Phys. **11**, 728 (2015).

[88] Hao Zheng *et al.*, Atomic-scale visualization of quantum interference on a Weyl semimetal surface by scanning tunneling microscopy, ACS Nano **10**, 1378 (2016).

[89] P. Hosur and X. Qi, Recent developments in transport phenomena in Weyl semimetals, C. R. Phys. **14**, 857 (2013).

[90] Huichao Wang and Jian Wang, Electron transport in Dirac and Weyl semimetals, Chin. Phys. B **27**, 107402 (2018).

[91] Jin Hu, Su-Yang Xu, Ni Ni, and Zhiqiang Mao, Transport of topological semimetals, Annu. Rev. Mater. Res. **49**, 207 (2019).

[92] A. A. Zyuzin and A. A. Burkov, Topological response in Weyl semimetals and the chiral anomaly, Phys. Rev. B **86**, 115133 (2012).

[93] Y. Chen, Si Wu, and A. A. Burkov, Axion response in Weyl semimetals, Phys. Rev. B **88**, 125105 (2013).

[94] M. M. Vazifeh and M. Franz, Electromagnetic Response of Weyl Semimetals, Phys. Rev. Lett. **111**, 027201 (2013).

[95] A. A. Burkov, Chiral anomaly and transport in Weyl metals, J. Phys. Condens. Matter **27**, 113201 (2015).

[96] P. Hosur, S. A. Parameswaran, and A. Vishwanath, Charge Transport in Weyl Semimetals, Phys. Rev. Lett. **108** (2012).

[97] Fernando de Juan, Adolfo G. Grushin, Takahiro Morimoto, and Joel E. Moore, Quantized circular photogalvanic effect in Weyl semimetals, Nat. Commun. **8**, 15995 (2017).

[98] Shuo Wang, Ben Chuan Lin, An Qi Wang, Da Peng Yu, and Zhi Min Liao, Quantum transport in Dirac and Weyl semimetals: A review, Adv. Phys. X **2**, 518 (2017).

[99] Naoto Nagaosa, Takahiro Morimoto, and Yoshinori Tokura, Transport, magnetic and optical properties of Weyl materials, Nat. Rev. Mater. **5**, 621 (2020).

[100] H. B. Nielsen and M. Ninomiya, The Adler-Bell-Jackiw anomaly and Weyl fermions in a crystal, Phys. Lett. B **130**, 389 (1983).

[101] M. V. Isachenkov and A. V. Sadofyev, The chiral magnetic effect in hydrodynamical approach, Phys. Lett. B **697**, 404 (2011).

[102] A. V. Sadofyev, V. I. Shevchenko, and V. I. Zakharov, Notes on chiral hydrodynamics within the effective theory approach, Phys. Rev. D **83**, 105025 (2011).

[103] R. Loganayagam and Piotr Surówka, Anomaly/transport in an Ideal Weyl gas, J. High Energy Phys. 04 (2012) 097.

[104] Pallab Goswami and Sumanta Tewari, Axionic field theory of $(3 + 1)$-dimensional Weyl semimetals, Phys. Rev. B **88**, 245107 (2013).

[105] Zhong Wang and Shou-Cheng Zhang, Chiral anomaly, charge density waves, and axion strings from Weyl semimetals, Phys. Rev. B **87**, 161107(R) (2013).

[106] G. Basar, Dmitri E. Kharzeev, and Ho-Ung Yee, Triangle anomaly in Weyl semimetals, Phys. Rev. B **89**, 035142 (2014).

[107] Karl Landsteiner, Anomalous transport of Weyl fermions in Weyl semimetals, Phys. Rev. B **89**, 075124 (2014).

[108] Swadeepan Nanda and Pavan Hosur, Vortical effects in chiral band structures, arXiv:2206.14194.

[109] Enrique Benito-Matías and Rafael A. Molina, Surface states in topological semimetal slab geometries, Phys. Rev. B **99**, 075304 (2019).

[110] Peng Deng, Zhilin Xu, Ke Deng, Kenan Zhang, Yang Wu, Haijun Zhang, Shuyun Zhou, and Xi Chen, Revealing

Fermi arcs and Weyl nodes in MoTe2 by quasiparticle interference mapping, Phys. Rev. B **95**, 245110 (2017).
[111] Ke Deng *et al.*, Experimental observation of topological Fermi arcs in type-II Weyl semimetal MoTe2, Nat. Phys. **12**, 1105 (2016).
[112] F. D. M. Haldane, Attachment of surface "Fermi Arcs" to the bulk fermi surface: "Fermi-Level Plumbing" in topological metals, 2014.
[113] P. Hosur, Friedel oscillations due to Fermi arcs in Weyl semimetals, Phys. Rev. B **86**, 195102 (2012).
[114] Lunan Huang, Timothy M. McCormick, Masayuki Ochi, Zhiying Zhao, Michi To Suzuki, Ryotaro Arita, Yun Wu, Daixiang Mou, Huibo Cao, Jiaqiang Yan, Nandini Trivedi, and Adam Kaminski, Spectroscopic evidence for a type II Weyl semimetallic state in MoTe 2, Nat. Mater. **15**, 1155 (2016).
[115] Davide Iaia, Guoqing Chang, Tay-Rong Chang, Jin Hu, Zhiqiang Mao, Hsin Lin, Shichao Yan, and Vidya Madhavan, Searching for topological Fermi arcs via quasiparticle interference on a type-II Weyl semimetal MoTe2, npj Quantum Mater. **3**, 38 (2018).
[116] Hyeokshin Kwon, Taehwan Jeong, Samudrala Appalakondaiah, Youngtek Oh, Insu Jeon, Hongki Min, Seongjun Park, Young Jae Song, Euyheon Hwang, and Sungwoo Hwang, Quasiparticle interference and impurity resonances on WTe2, Nano Res. **13**, 2534 (2020).
[117] Alexander Lau, Klaus Koepernik, Jeroen Van Den Brink, and Carmine Ortix, Generic Coexistence of Fermi Arcs and Dirac Cones on the Surface of Time-Reversal Invariant Weyl Semimetals, Phys. Rev. Lett. **119**, 076801 (2017).
[118] M. Sakano, M. S. Bahramy, H. Tsuji, I. Araya, K. Ikeura, H. Sakai, S. Ishiwata, K. Yaji, K. Kuroda, A. Harasawa, S. Shin, and K. Ishizaka, Observation of spin-polarized bands and domain-dependent Fermi arcs in polar Weyl semimetal MoTe2, Phys. Rev. B **95**, 121101 (2017).
[119] Su Yang Xu *et al.*, Experimental discovery of a topological Weyl semimetal state in TaP, Sci. Adv. **1** (2015).
[120] Su Yang Xu *et al.*, Observation of Fermi arc surface states in a topological metal, Science **347**, 294 (2015).
[121] Qiunan Xu, Enke Liu, Wujun Shi, Lukas Muechler, Jacob Gayles, Claudia Felser, and Yan Sun, Topological surface Fermi arcs in the magnetic Weyl semimetal Co3Sn2S, Phys. Rev. B **97**, 235416 (2018).
[122] Yuan Yuan, Xing Yang, Lang Peng, Zhi-Jun Wang, Jian Li, Chang-Jiang Yi, Jing-Jing Xian, You-Guo Shi, and Ying-Shuang Fu, Quasiparticle interference of Fermi arc states in the type-II Weyl semimetal candidate WTe2, Phys. Rev. B **97**, 165435 (2018).
[123] Qian-Qian Yuan, Liqin Zhou, Zhi-Cheng Rao, Shangjie Tian, Wei-Min Zhao, Cheng-Long Xue, Yixuan Liu, Tiantian Zhang, Cen-Yao Tang, Zhi-Qiang Shi, Zhen-Yu Jia, Hongming Weng, Hong Ding, Yu-Jie Sun, Hechang Lei, and Shao-Chun Li, Quasiparticle interference evidence of the topological Fermi arc states in chiral fermionic semimetal CoSi, Sci. Adv. **5**, aaw948 (2019).
[124] Cheng Zhang, Awadhesh Narayan, Shiheng Lu, Jinglei Zhang, Huiqin Zhang, Zhuoliang Ni, Xiang Yuan, Yanwen Liu, Ju-Hyun Park, Enze Zhang, Weiyi Wang, Shanshan Liu, Long Cheng, Li Pi, Zhigao Sheng, Stefano Sanvito, and Faxian Xiu, Evolution of Weyl orbit and quantum Hall effect in Dirac semimetal Cd3As2, Nat. Commun. **8**, 1272 (2017).
[125] Philip J. W. Moll, Nityan L. Nair, Toni Helm, Andrew C. Potter, Itamar Kimchi, Ashvin Vishwanath, and James G. Analytis, Transport evidence for Fermi-arc-mediated chirality transfer in the Dirac semimetal Cd3As2, Nature (London) **535**, 266 (2016).
[126] Andrew C Potter, Itamar Kimchi, and Ashvin Vishwanath, Quantum oscillations from surface Fermi arcs in Weyl and Dirac semimetals, Nat. Commun. **5**, 5161 (2014).
[127] Y. Zhang, D. Bulmash, P. Hosur, A. C. Potter, and A. Vishwanath, Quantum oscillations from generic surface Fermi arcs and bulk chiral modes in Weyl semimetals, Sci. Rep. **6** (2016).
[128] Yi Li and F. D. M. Haldane, Topological Nodal Cooper Pairing in Doped Weyl Metals, Phys. Rev. Lett. **120**, 067003 (2018).
[129] Gil Young Cho, Jens H. Bardarson, Yuan-Ming Lu, and Joel E. Moore, Superconductivity of doped Weyl semimetals: Finite-momentum pairing and electronic analog of the ^{3}He-A phase, Phys. Rev. B **86**, 214514 (2012).
[130] Huazhou Wei, Sung-Po Chao, and Vivek Aji, Odd-parity superconductivity in weyl semimetals, Phys. Rev. B **89**, 014506 (2014).
[131] Lei Hao, Rui Wang, Pavan Hosur, and C. S. Ting, Larkin-Ovchinnikov state of superconducting Weyl metals: Fundamental differences between restricted and extended pairings in k-space, Phys. Rev. B **96**, 094530 (2017).
[132] Rauf Giwa and Pavan Hosur, Fermi Arc Criterion for Surface Majorana Modes in Superconducting Time-Reversal Symmetric Weyl Semimetals, Phys. Rev. Lett. **127**, 187002 (2021).
[133] Ashvin Vishwanath, Vortices, quasiparticles and unconventional superconductivity, Ph.D. thesis, Princeton University, 2001.
[134] See Supplemental Material at http://link.aps.org/supplemental/10.1103/PhysRevLett.130.156402 for (i) an analytical calculation of ϕ_Q in an ideal limit; (ii) description of Majorana modes, SUSY, magic angle, and a symmetry principle for a materials search; (iii) the lattice model, an elegant analytical calculation of ϕ_S in the model, and details of the numerical fits, 2022.
[135] Ching Kai Chiu, Jeffrey C. Y. Teo, Andreas P. Schnyder, and Shinsei Ryu, Classification of topological quantum matter with symmetries, Rev. Mod. Phys. **88**, 035005 (2016).
[136] K. T. Law, Patrick A. Lee, and T. K. Ng, Majorana Fermion Induced Resonant Andreev Reflection, Phys. Rev. Lett. **103**, 237001 (2009).
[137] Haining Pan, Chun-Xiao Liu, Michael Wimmer, and Sankar Das Sarma, Quantized and unquantized zero-bias tunneling conductance peaks in majorana nanowires: Conductance below and above $2e^2/h$, Phys. Rev. B **103**, 214502 (2021).
[138] Y. Ran, P. Hosur, and A. Vishwanath, Fermionic Hopf solitons and Berry phase in topological surface superconductors, Phys. Rev. B **84**, 184501 (2011).

[139] Daniel Friedan, Zongan Qiu, and Stephen Shenker, Superconformal invariance in two dimensions and the tricritical ising model, Phys. Lett. B **151**, 37 (1985).
[140] Xiao-Liang Qi, Taylor L. Hughes, S. Raghu, and Shou-Cheng Zhang, Time-Reversal-Invariant Topological Superconductors and Superfluids in Two and Three Dimensions, Phys. Rev. Lett. **102**, 187001 (2009).
[141] Shengshan Qin, Lunhui Hu, Congcong Le, Jinfeng Zeng, Fu-chun Zhang, Chen Fang, and Jiangping Hu, Quasi-1D Topological Nodal Vortex Line Phase in Doped Superconducting 3D Dirac Semimetals, Phys. Rev. Lett. **123**, 027003 (2019).
[142] Zhongbo Yan, Zhigang Wu, and Wen Huang, Vortex End Majorana Zero Modes in Superconducting Dirac and Weyl Semimetals, Phys. Rev. Lett. **124**, 257001 (2020).
[143] Elio J. Konig, Piers Coleman, Elio J. König, and Piers Coleman, Crystalline-Symmetry-Protected Helical Majorana Modes in the Iron Pnictides, Phys. Rev. Lett. **122**, 207001 (2019).
[144] Tiantian Zhang, Yi Jiang, Zhida Song, He Huang, Yuqing He, Zhong Fang, Hongming Weng, and Chen Fang, Catalogue of topological electronic materials, Nature (London) **566**, 475 (2019).
[145] M. G. Vergniory, L. Elcoro, Claudia Felser, Nicolas Regnault, B. Andrei Bernevig, and Zhijun Wang, A complete catalogue of high-quality topological materials, Nature (London) **566**, 480 (2019).
[146] Feng Tang, Hoi Chun Po, Ashvin Vishwanath, and Xiangang Wan, Comprehensive search for topological materials using symmetry indicators, Nature (London) **566**, 486 (2019).
[147] Jan Borchmann and T. Pereg-Barnea, Quantum oscillations in Weyl semimetals: A surface theory approach, Phys. Rev. B **96**, 125153 (2017).
[148] Chi-Cheng Lee, Su-Yang Xu, Shin-Ming Huang, Daniel S. Sanchez, Ilya Belopolski, Guoqing Chang, Guang Bian, Nasser Alidoust, Hao Zheng, Madhab Neupane, Baokai Wang, Arun Bansil, M. Zahid Hasan, and Hsin Lin, Fermi surface interconnectivity and topology in Weyl fermion semimetals taas, TaP, NbAs, and NbP, Phys. Rev. B **92**, 235104 (2015).
[149] S. Souma, Zhiwei Wang, H. Kotaka, T. Sato, K. Nakayama, Y. Tanaka, H. Kimizuka, T. Takahashi, K. Yamauchi, T. Oguchi, Kouji Segawa, and Yoichi Ando, Direct observation of nonequivalent fermi-arc states of opposite surfaces in the noncentrosymmetric Weyl semimetal NbP, Phys. Rev. B **93**, 161112 (2016).
[150] H. Suderow, I. Guillamón, J. G. Rodrigo, and S. Vieira, Imaging superconducting vortex cores and lattices with a scanning tunneling microscope, Semicond. Sci. Technol. **27**, 063001 (2014).